Stretching the Boundary: Shell Finite Elements for Pneumatic Soft Actuators

Lawrence Smith[1], Jacob Haimes[1], Robert MacCurdy[1*]

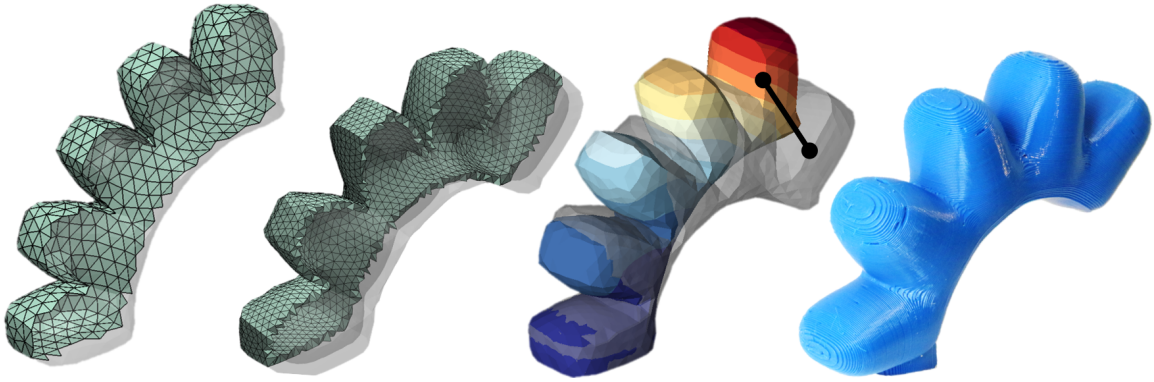

From left: simulated response to internal pneumatic loading using shell and volumetric finite element analysis, respectively; superposition of deformed geometry with contours showing L2 norm of local difference in position estimate between the simulations; 3D-printed soft actuator.

***Abstract*— Many soft robotics researchers use numerical simulation; all of them wish their simulations would run faster. In this paper we highlight an attractive option for simulating pneumatic soft actuator designs: zero-thickness shell finite elements. These offer a favorable balance between predictive accuracy and computational cost relative to standard approaches. We find that shell finite elements offer a 7x reduction in analysis time while accurately predicting the behavior of a wide variety of soft actuators. The benefits conferred by shell finite element analysis are especially valuable in contexts where simulation speed is as important as absolute accuracy, such as automated design, optimization, and real-time control.**

I. Introduction

Soft robotics researchers navigate a challenging design space relying largely on intuition developed over time-consuming design/build/test cycles. Predictive numerical simulations offer valuable design insights with significant time savings - yet access to consistent, accurate, and efficient simulation results remains an aspiration, not a reality for many research efforts. Popular simulation methods require impractical amounts of computation time and setup [1], and bottlenecks exist between software tools used for design, simulation, and fabrication of soft actuators. Our recent work proposes an alternative paradigm that facilitates soft actuator synthesis through indirect encodings to create implicit functional geometry representations which can be readily simulated and fabricated using interactive computer aided design (CAD) tools [2]. An advantage of this method is the trivial extraction of zero thickness triangulations of an actuator's outer boundary at arbitrary resolution, which may be immediately used as a computational mesh. In this paper, we advocate for the use of shell finite elements for simulating pneumatic soft actuators, especially during early phases of design exploration.

[1]Authors are with the Department of Mechanical Engineering, University of Colorado Boulder, Boulder, CO, USA

* Corresponding author: *maccurdy@colorado.edu*

A. Shell Finite Elements

We use shell finite elements for the same reason that dimensional reduction in structural analysis has been used for centuries [3]: to reduce the complexity of a problem and focus on the essentials. Shells are three dimensional structures having one dimension (the thickness) much smaller than the other two. Shells are some of the most common construction elements in nature and human technology across length scales; cell walls, invertebrate bodies, architectural domes, fuselages, and automobile exteriors are a few examples.

Shell finite elements consider solution quantities constant through the thickness dimension and integrate material properties to produce zero-thickness representations of shell structures with stiffness in tension, compression, shear, and bending. Due to to their outstanding utility in structural analysis, many variations of shell finite elements have been implemented in both commercial (e.g. *Abaqus*) and open-source (e.g. FEBio [4], MOOSE [5]) software, including variants specialized for small and large deformations, multi-scale and multiphysics problems, buckling, composites, and higher-order formulation [3].

However, this dimensional reduction comes with a cost: shell elements exhibit numerical locking, predicting artificially higher stiffness than do solid finite elements. This phenomenon is most severe in bending-dominated loading scenarios, when the shell thickness to span ratio falls below 1:10, or when element quality is poor. Extensive study [6] has attempted to quantify this effect and offered mitigations, such as selective reduced integration (SRI) element formulations, guidelines for mesh patterns, and elements with additional bending degrees of freedom at each node.

When discretizing thin-wall, large-span structures, many small volumetric finite elements must be used in order to preserve element quality (Figure 1, right). Shell meshes can represent the same geometry using fewer elements

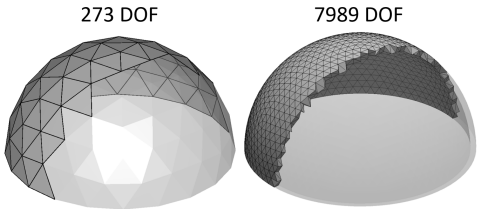

Fig. 1. Shell meshes (left) represent thin structures using significantly fewer finite elements. In order to preserve element quality in the volumetric mesh (right), tetrahedral edge length must be kept roughly equal to wall thickness, resulting in an order of magnitude increase in degrees of freedom (DOF).

while maintaining excellent element quality. Algorithms for automatically generating and regularizing triangular and quadrilateral [7] shell meshes exist; automated hexahedral mesh generation on arbitrary geometries remains an open problem despite enormous research effort [8]. In this paper, we formalize an argument that is implicit in the continued use of shell finite elements for many other engineering problems: on balance, the advantages conferred by shell finite elements in soft actuator analysis outweigh potential downsides.

B. Simulation in Soft Robotics

The tension between simulation computational cost and predictive accuracy is well-studied, and key works in soft robotics literature each strike their own balance. Table I collects significant soft robotics results with a simulation component. By far the most common approach for simulating soft robot designs is nonlinear finite element analysis (FEA) in 3 dimensions [9] using either tetrahedral or hexahedral volumetric finite elements, as in Table I, left column. These simulations accurately predict empirical responses for a variety of complex geometries under varied loading.

Next most common in the literature are examples of dimensional reduction to 1D, yielding *beam*/*rod* models. Whether analytical or finite element based, these models are appropriate only for long, slender geometries, in which two spatial dimensions are much smaller than the third. These models capture the shape of a deformed finger as well as a one-dimensional model can, and are accepted as sufficiently accurate for trajectory planning and control [10]. 1D models have significant shortcomings for design exploration; fundamental relationships between model inputs (e.g. material distribution, applied pressure) and curvature are often heuristic or require experimental data to extrapolate from, and they are suited strictly for rod-shaped geometries.

TABLE I: Dimension Reduction in Soft Actuator Analysis

3D (unreduced)	2D (shell)	1D (beam/rod)	0D (lumped)
[11] [12] [13] [14] [15] [16] [17] [18] [19] [5]	[2] [20]	[21] [22] [23] [24] [25] [10] [26] [27] [28] [18] [29]	[30] [31]

The advantage of a 1D model is exceptional reduction in computational cost in comparison to a 3D FEA model, allowing for faster than real-time simulation execution. Curiously, very few examples of dimensional reduction to 2D elements can be found in literature - even though this seems a natural intermediate step between expensive yet general 3D models and lightweight but limited 1D models.

Finally, examples of soft robot simulation using lumped models not derived from continuum theory exist, such as the notable [30] and [31]. These efforts show the utility of relaxing accuracy requirements in order to achieve incredibly fast runtimes - in both cases enabling sprawling gradient-free optimization experiments that have not been replicated using more conventional, computationally expensive simulation.

II. Methods

A. Computational Mesh Formation

In this study we simulate actuators represented by implicit geometry functions. Evaluating these functions over a spatial domain produces a scalar field, from which we can extract a zero-thickness isosurface representing the outer boundary of the actuator. We use the Geometry and Image-Based Bioengineering add-On (GIBBON) [32] to create high-quality triangular shell finite element meshes of these isosurfaces. All computational meshes are assigned a wall thickness of $1.6\,\text{mm}$, a realistic value used for fabricating soft actuators with additive manufacturing.

To generate volumetric meshes, we extract a second (interior) surface offset from the outer boundary by a constant distance. We use the open source software *TetGen* [33] to generate tetrahedral meshes between these bounding surfaces, with an average element edge length equal to the wall thickness. This produces a computational mesh that is as coarse as possible for simulating these geometries using volumetric elements.

B. Finite Element Analysis

We simulate all geometries using nonlinear quasistatic FE analysis with the commercial package *Abaqus*. We use parameters for the Ogden hyper-elastic material model taken from [17] for all simulations, listed in Table II. We remove all degrees of freedom from a group of nodes at one end of the actuator (to simulate an external attachment) and apply a pressure load to all internal faces, which increases in magnitude until the simulation loses stability. All studies use full Newton incrementation and we allow default selection of pseudotimestep for application of internal pressure.

C. Computational Cost

Computational cost is the wallclock time to perform analysis, broken into subtasks for mesh formation, finite element analysis, and post processing (reading data from output files). All simulations are performed on identical hardware: a fast but affordable desktop PC with an AMD Ryzen 3900x CPU (24 threads, 4.1 GHz) and 64 GB of RAM. We did not enable multithreading or GPU acceleration for this study.

TABLE II: FEA Model Parameters

Mesh	**Element**	**Ogden Parameters**			
Solid	Linear Tet C3D4H	μ_1	-30.921	α_1	0.508
Shell	Linear Tri SR3	μ_2	10.342	α_2	1.375
		μ_3	26.791	α_3	-0.482

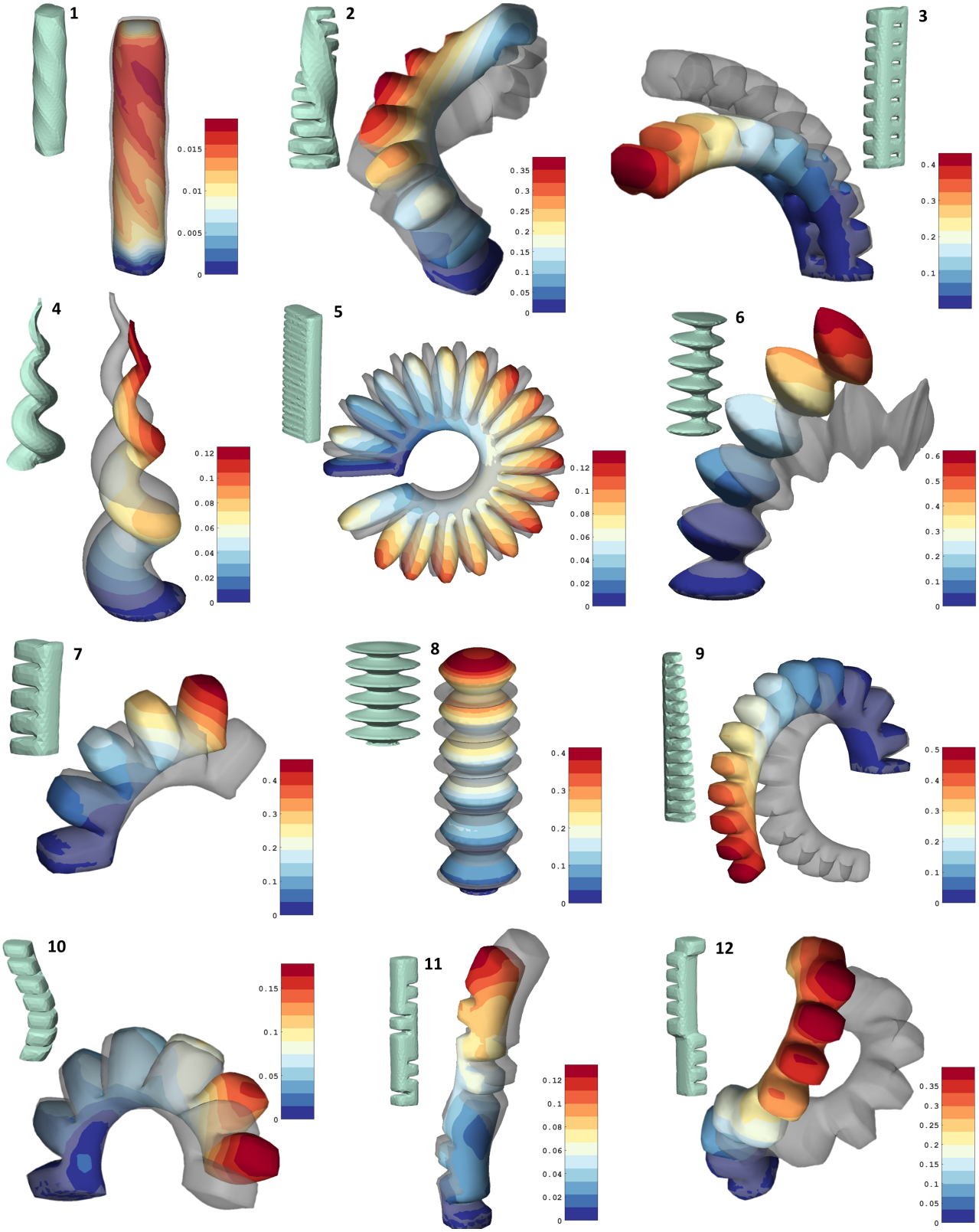

Fig. 2. Selection of twelve soft actuator designs simulated using shell (color) and tetrahedral (transparent) finite element meshes. Insets show the un-actuated designs. Color contours show L2 norm of local difference in position as predicted by the two simulations, normalized by the undeformed length of the actuator. In these simulations we remove all degrees of freedom from a group of nodes at one end of the actuator and apply a quasistatic pressure load to all internal faces. Mesh and material model data are given in Table II. These actuators exhibit bending, twisting, and extension modes of deformation, and shell meshes capture the deformation shapes well. As expected, shell meshes are less compliant at equivalent pressure due to numerical locking, however the trajectories of the deformation are remarkably similar. Generation of shell and volume meshes, as well as simulation execution and post-processing, is fully automated. The color map used in these plots originates from ColorBrewer [34]. All designs are represented by implicit geometry functions available for download: https://www.matterassembly.org/soft-actuator-synthesis.

D. Accuracy Measure

In order to quantify accuracy of shell finite element results relative to volumetric FEA, we compute local difference in position of the outer surface of each mesh. In the undeformed configuration, we create a mapping between each node in the shell mesh and the nearest node on the surface of the volumetric mesh. At specified load increments we interpolate the deformation field of each study and then compute the difference in position of the nodes across this mapping. We normalize this distance by the length of the actuator, and report local L2 norm of the distance using color contours.

III. Results

We compare accuracy and speed metrics across a selection of twelve soft actuator designs visualized in Figure 2. This selection exhibits a wide variety of responses when internal pressure is applied, including bending, twisting, extension, and compound motions reminiscent of many published soft actuator results [35]. We note an average speedup of 7x when using shell finite elements (Table III), and that shell simulations capture the deformation behavior seen in the more computationally expensive volumetric (hereafter "reference") simulations.

TABLE III: Speed Comparison (Reference/Shell) [s]

Design Number	Mesh and Process	FEA Solve	Total (speed-up)	
1	37/3	221/32	133/35	(3.8x)
2	246/10	403/112	649/122	(5.3x)
3	114/6	400/62	514/68	(7.6x)
4	123/4	178/42	301/47	(6.4x)
5	178/30	771/220	950/251	(3.8x)
6	117/8	346/73	524/82	(6.4x)
7	50/4	219/50	267/55	(4.9x)
8	906/11	687/102	1591/112	(14.2x)
9	89/12	344/101	434/114	(3.9x)
10	253/16	671/132	92/149	(6.2x)
11	113/7	265/65	378/73	(10.1x)
12	140/9	397/76	537/85	(6.3x)

As expected, simulations over shell meshes exhibit more numerical locking than their volumetric counterparts in reference simulations, predicting higher stiffness in all twelve cases we explored. However, the deformation modes predicted by the shell simulations are nearly identical to reference. In other words, shell simulations reliably predict qualitative actuator behavior. Frequency analysis (Figure 3) highlights this - mode shapes predicted by FE analysis over shell and reference meshes are exceptionally similar.

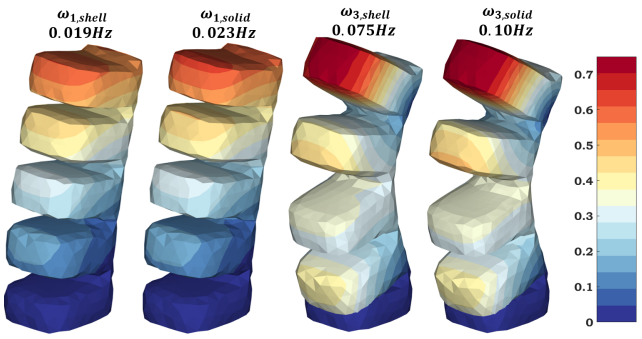

Fig. 3. Mode shapes of actuator 7 as predicted by frequency analysis using shell and volumetric elements. Mode shapes are intrinsic to actuator geometry and material composition and do not depend on loading conditions. Contours show normalized displacement magnitude.

We can improve agreement between shell and reference simulations by posing minimization of the L2 norm plotted in Figure 2 as an optimization problem, subject to linear scaling of the pressure applied to the shell mesh. We perform this analysis on all actuators (Table IV) using *Matlab's* native *fminsearch()* function, and find that scaling the nominal load applied to the shell mesh can bring shell simulations into close agreement with reference simulations (Figure 4), delivering a mean reduction in error measure of 6x over nominal loads. However, the optimal scaling factor varies across actuators - see Section IV for further discussion.

TABLE IV: Pressure Scaling Effects

Design	Scaling Factor	Nominal/Scaled $\int \|e\| dA$ (Reduction)
1	2.43	0.124/0.017 (9.0x)
2	1.69	0.224/0.057 (3.9x)
3	1.20	0.075/0.010 (7.6x)
4	2.18	0.234/0.026 (8.9x)
5	1.10	0.034/0.033 (1.0x)
6	2.19	0.305/0.169 (1.8x)
7	1.93	0.432/0.050 (8.7x)
8	1.52	0.095/0.015 (6.5x)
9	1.49	0.346/0.059 (5.9x)
10	1.22	0.171/0.058 (2.9x)
11	1.83	0.182/0.053 (3.5x)
12	1.78	0.416/0.023 (18.2x)

Load scaling calibration reduces shell simulation error. Rightmost column reports normalized global error (integrated local error divided by area).

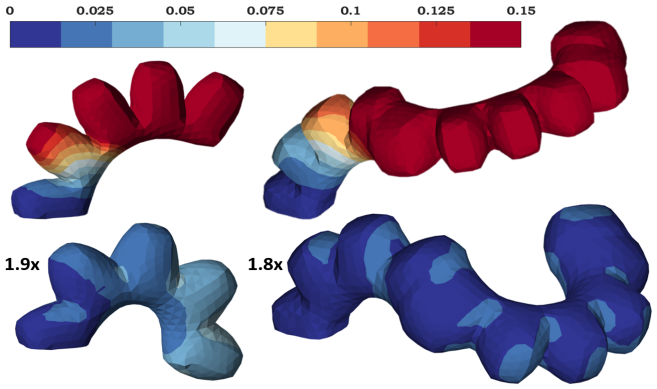

Fig. 4. Load scaling on shell FE simulations reduces error relative to reference simulations. Contours are L2 norm of local difference in displacement field from reference for nominal (upper) and scaled (lower) pressure loads in shell simulations of actuators 7 (left) and 12 (right)

Finally, because the designs analyzed here are represented by implicit functions, we can trivially extract computational meshes of abitrary resolution and investigate effects of mesh refinement. We re-simulate the actuator selection shown in Figure 2 using tetrahedral elements with average edge length reduced by half. These simulations are expensive, requiring an average of 32.6x longer to execute than shell element simulations. They also exhibit higher deflections at

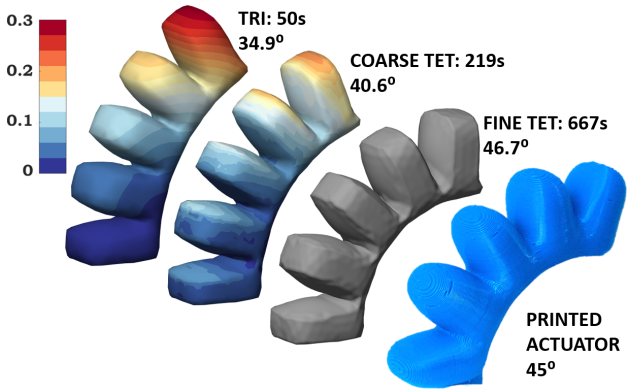

Fig. 5. Shell elements capture deformation modes relative to reference simulations and reality. From back to foreground: shell finite element simulation, reference coarse tet simulation, fine tet simulation, fabricated (3D-printed) actuator design #7.

equivalent loads than both the shell and reference simulations (e.g. Figure 5), likely due to reduced numerical locking and accuracy improvements associated with mesh refinement. These simulations underline the tradeoff between predictive accuracy and computational cost that is core to numerical simulation of soft actuators.

A. Special Considerations

1) Nonuniform Shells: Many pneumatic soft actuators achieve desired motions by controlling local material properties - for example, inducing bending behavior by placing an inextensible layer on one side of an actuator [11]. Local control over material properties and wall thickness may be trivially achieved in shell finite element analysis by modifying shell properties on an element-by-element basis. Finer control can be exercised if material and/or wall thickness properties are available as analytical fields - these fields can be evaluated at each element's Gauss points during local stiffness matrix formation, allowing for intra-element variation in properties [36].

2) Pressure Boundary Conditions: In defining a zero-thickness shell element mesh, practitioners must decide where to place that surface relative to the original inner and outer surfaces of a 3D geometry. In this work, we make the shell mesh coincident with the outer surface of the original 3D actuator, preserving the contact boundary. One could alternatively place the shell mesh on the interior surface of the 3D geometry, or at the midsurface - each leads to small differences in the geometry which is loaded by internal pressure and/or presented to the environment.

By placing the shell mesh on the exterior of the actuator, we slightly increase the total area on which an internal pressure load acts. Additionally, in regions where the length scale of geometric features is similar to the wall thickness, the interior and exterior surfaces may diverge significantly in geometry and even topology - note the tip of the spiral actuator in Figure 6, which is completely solid. In order to most closely resemble the pressurization of an actual 3D actuator, shell boundary conditions can be adjusted to omit loading on shell faces which are not nearby to the actuator's inner wall surface. This condition can be trivially detected

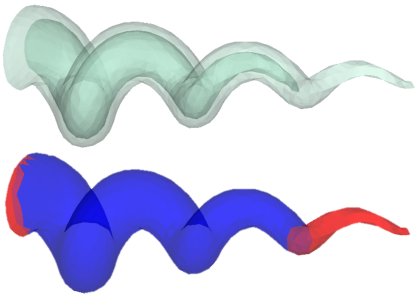

Fig. 6. Shell mesh (lower), with automatic detection of faces excluded from pressure load set to account for closed areas of original geometry (upper).

in actuators represented by implicit geometry functions; we simply examine the signed distance field associated with the inner surface of the actuator.

3) Contact Boundary Conditions: Soft robots excel in interaction with dynamic and uncertain environments, such as grasping irregularly shaped objects. The most general technique for handling interactions with the environment in simulation is by modelling contact at the exterior boundaries of participating bodies. Contact is handled at the level of surfaces, so simulation with shell finite elements does not confer any specific benefits here, except that the discretization at the contact boundaries can usually be coarser than in a corresponding tetrahedral mesh, leading to fewer boundary condition nonlinearity terms.

We test the performance of shell finite elements in a contact scenario by simulating a bending soft actuator interacting with a stationary contact surface offset from the underside of the actuator (Figure 7). The actuator simulated with shell elements transmits more force to the contact surface at equivalent pressures - we attribute this result to the increased stiffness of the shell actuator, which prevents deformation away from the contact plane.

IV. Conclusions

We find that simulations on shell meshes present a 7x average reduction in computational cost, as well as clear time savings in the generation of computational meshes and the post-processing of results. As expected, shell finite element simulations under-predict deformations relative to reference analyses due to known numerical locking issues which are especially pronounced for linear triangular shell elements. We find that shell elements predict deformations with a normalized error typically less than 20 % of the length of the actuator. However, the modal behavior and deformations under load predicted by shell finite element simulations are remarkably similar to the results of reference simulations - albeit requiring more pressure to achieve them. This is critical to the thesis of this paper for two reasons.

First, for any given actuator, a scaling argument can reasonably be made, and the agreement between the simulations can be improved by scaling the pressure applied to the shell simulation. This scaling factor is a function of actuator geometry, material properties, and mesh resolution, and is best determined on a case-by-case basis. Where this scaling characterization can be performed "offline," (for example,

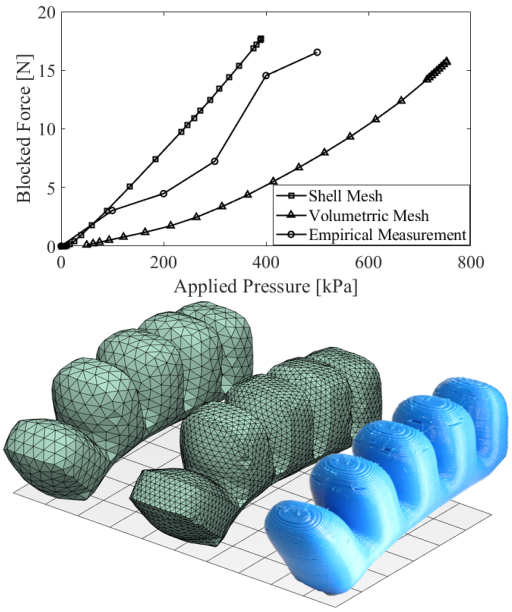

Fig. 7. Actuator #7 simulated in a blocked force scenario with triangular shell elements (left), tetrahedral solid elements (middle), 3D printed (right). Simulations executed in 233 s and 606 s for the shell and solid meshes, respectively. The more compliant tet mesh transmits less force at equivalent pressure (top).

FEA-based control [1] [37]), shell elements offer attractive time savings. Furthermore, the magnitude of applied pressure in an application is typically the subject of subsequent controller design steps, after the actuator design has been established. These steps include a sim-to-real closure, during which the magnitude error would be corrected. Despite the deformation magnitude errors detailed in Table IV, Figure 5 shows remarkable correspondence between shell-element simulation and an actual 3D-printed actuator.

Second, certain soft robotics applications do not require absolute accuracy of simulation results, only relative accuracy as compared to other results generated with the same simulation method. Automated design is an excellent example - particularly early in a design experiment, when rapid exploration of the design space can be especially valuable. This iterative process requires many simulations of candidate solutions, and often compares the performance of those designs to other candidates on a relative basis. Shell elements provide an inexpensive means to predict the behavior of soft actuators, and can enable automated design algorithms to explore a design space more rapidly than using traditional volumetric elements would allow. Towards the end of an automated design effort, designers may chose to put a premium on absolute accuracy and switch to using volumetric elements at the cost of longer simulation times.

References

[1] M. Pozzi *et al.*, "Efficient FEM-Based simulation of soft robots modeled as kinematic chains," *Proceedings - IEEE International Conference on Robotics and Automation*, 2018.

[2] L. Smith *et al.*, "A Seamless Workflow for Design and Fabrication of Multimaterial Pneumatic Soft Actuators," 2021.

[3] M. Bischoff *et al.*, "Models and Finite Elements for Thin-Walled Structures," *Encyclopedia of Computational Mechanics*, 2004.

[4] S. Maas *et al.*, "FEBio: Finite elements for biomechanics," *Journal of Biomechanical Engineering*, 2012.

[5] K. Wandke, "MOOSE-based Finite Element Hyperelastic Modeling for Soft Robot Simulations," *IEEE Access*, 2021.

[6] P. Lee, H. C. Noh, and K. J. Bathe, "Insight into 3-node triangular shell finite elements: the effects of element isotropy and mesh patterns," *Computers and Structures*, 2007.

[7] J. Docampo-s and R. Haimes, "A Regularization Approach For Automatic Quad Mesh Generation," 2021.

[8] G. Joldes, A. Wittek, and K. Miller, "Suite of finite element algorithms for accurate computation of soft tissue deformation for surgical simulation," *Medical Image Analysis*, 2009.

[9] D. Holland *et al.*, "The Soft Robotics Toolkit: Shared Resources for Research and Design," *Soft Robotics*, 2014.

[10] J. Till and D. Rucker, "Elastic stability of cosserat rods and parallel continuum robots," *IEEE Transactions on Robotics*, 2017.

[11] B. Mosadegh *et al.*, "Pneumatic networks for soft robotics that actuate rapidly," *Advanced Functional Materials*, 2014.

[12] L. Ding *et al.*, "Design of soft multi-material pneumatic actuators based on principal strain field," *Materials and Design*, 2019.

[13] M. Schaffner *et al.*, "3D printing of robotic soft actuators with programmable bioinspired architectures," *Nature Communications*, 2018.

[14] C. Pasquier *et al.*, "Design and Computational Modeling of a 3D Printed Pneumatic Toolkit for Soft Robotics," 2019.

[15] T. Hainsworth *et al.*, "A Fabrication Free, 3D Printed, Multi-material, self-sensing soft actuator," *IEEE Robotics & Automation Letters*, 2020.

[16] W. Xiao *et al.*, "A new type of soft pneumatic torsional actuator with helical chambers for flexible machines," *Journal of Mechanisms and Robotics*, 2021.

[17] H. Yap, H. Y. Ng, and C. H. Yeow, "High-Force Soft Printable Pneumatics for Soft Robotic Applications," *Soft Robotics*, 2016.

[18] G. Zhong *et al.*, "Bending analysis and contact force modeling of soft pneumatic actuators with pleated structures," *International Journal of Mechanical Sciences*, 2021.

[19] S. Wakimoto, K. Suzumori, and K. Ogura, "Miniature pneumatic curling rubber actuator generating bidirectional motion with one air-supply tube," *Advanced Robotics*, 2011.

[20] P. Nguyen and W. Zhang, "Design and Computational Modeling of Fabric Soft Pneumatic Actuators for Wearable Assistive Devices," *Scientific Reports*, 2020.

[21] R. Webster and B. A. Jones, "Design and kinematic modeling of constant curvature continuum robots: A review," *International Journal of Robotics Research*, 2010.

[22] I. Gravagne, C. D. Rahn, and I. D. Walker, "Large deflection dynamics and control for planar continuum robots," *IEEE/ASME Transactions on Mechatronics*, 2003.

[23] "An Approach to Splitting Atoms Safely. Extended Abstract," *Electronic Notes in Theoretical Computer Science*, 2006.

[24] G. Gu *et al.*, "Analytical Modeling and Design of Generalized PneuNet Soft Actuators with Three-Dimensional Deformations," 2020.

[25] K. de Payrebrune and O. O'Reilly, "On constitutive relations for a rod-based model of a pneu-net bending actuator," *Extreme Mechanics Letters*, 2016.

[26] X. Liu *et al.*, "Soft humanoid hands with large grasping force enabled by flexible hybrid pneumatic actuators," *Soft Robotics*, 2021.

[27] X. Zhou, C. Majidi, and O. M. O'Reilly, "Soft hands: An analysis of some gripping mechanisms in soft robot design," *International Journal of Solids and Structures*, 2015.

[28] J. Till, V. Aloi, and C. Rucker, "Real-time dynamics of soft and continuum robots based on Cosserat rod models," *International Journal of Robotics Research*, 2019.

[29] I. Hussain *et al.*, "Modeling and Prototyping of a Soft Prosthetic Hand Exploiting Joint Compliance and Modularity," *IEEE International Conference on Robotics and Biomimetics, ROBIO*, 2019.

[30] N. Cheney *et al.*, "Unshackling evolution," *ACM SIGEVOlution*, 2014.

[31] G. Urbain *et al.*, "Morphological properties of mass-spring networks for optimal locomotion learning," *Frontiers in Neurorobotics*, 2017.

[32] K. Moerman, "GIBBON: The Geometry and Image-Based Bioengineering add-On," *The Journal of Open Source Software*, 2018.

[33] H. Si, "TetGen, a delaunay-based quality tetrahedral mesh generator," *ACM Transactions on Mathematical Software*, 2015.

[34] C. Brewer. (2013). [Online]. Available: https://colorbrewer2.org

[35] B. Gorissen *et al.*, "Elastic Inflatable Actuators for Soft Robotic Applications," *Advanced Materials*, 2017.

[36] E. Martínez-Pañeda, "On the finite element implementation of functionally graded materials," *Materials*, 2019.

[37] C. Duriez, "Control of elastic soft robots based on real-time finite element method," *Proceedings - IEEE International Conference on Robotics and Automation*, 2013.